An 3D face recognition approach based on facial curve analysis

Xuexian Hou*, Xinzhi Zhou, Yinjie Lei

School of Electronic Information, Sichuan University, Chengdu 610065, China

Abstract

In this paper, we present a novel 3D face recognition approach based on the analysis of facial curves, which are extracted from the semi-rigid facial regions. Our approach excludes the facial region which is most affected by facial expressions (non-rigid region) resulting in a set of indexed open geodesic curves. A novel open curve analysis algorithm combining the geodesic and Euclidean distances is used to match the same level pairs of open geodesic curves of a probe and the gallery faces. In order to increase the accuracy of face recognition, a curve ranking and weighting algorithm is also developed to select, during a training phase, the most reliable curves and to assign different weights to the selected ones. During the testing phase, the selected reliable curves and their corresponding distances are weighted fused to perform face recognition. The proposed approach has been tested on the Face Recognition Grand Challenge (FRGC v2.0) dataset via a number of experiments and a superior recognition performance was achieved.

Keywords: face recognition, facial curves, geodesic curves, FRGC v2.0

1 Introduction

2D face recognition has been an active research area in the past decades [1]. However, its recognition accuracy is adversely affected by pose and illumination variations, which makes it unsuitable for many practical applications. In order to overcome its inherent limitations and drawbacks, many researchers turned to 3D facial information, which revealed to have a greater potential to achieve a higher accuracy compared to just 2D [2].

In this work, we present a rigid 3D face recognition approach based on the matching of open facial curves. Based on our experimental results tested on the largest publicly available 3D face recognition dataset, Face Recognition Grand Challenge (FRGC v2.0), the proposed approach has shown to be effective for 3D face recognition under various facial expressions. In the literature, most of the related research is based on the analysis of closed facial curves [3-6]. The proposed approach uses open facial curves for the following two reasons. First, a facial surface comprises different expression-sensitive region (i.e. the mouth area is the most affected under facial expressions while the nose and eyes-forehead are the least affected). On that basis, and in order to eliminate the effect of facial expressions, we only use the upper region of the face (semi-rigid). This results in the extraction of open geodesic curves which are analyzed and matched to perform 3D face recognition. Second, according to the theory of Riemannian manifolds, the computation of the geodesic distance between open curves (used during the matching of the probe and gallery faces in our case) is much easier and time efficient compared to the distance between closed curves.

2 Related work and system overview

2.1 RELATED WORK

1) Facial curve analysis based approaches: This kind of approaches represent the 3D facial surfaces by a set of curves/strips which turns the task of matching 3D facial surfaces to the matching of 3D curves/strips. ter Haar et al. [7] introduced a 3D face matching framework based on 3D facial curves, which allowed profile and contour based face matching. A pair of corresponding curves was matched using point-to-point distance. Then a curve selection algorithm was applied to select subsets of the extracted facial curves in order to improve the effectiveness and efficiency of their face matching. In [6], Ballihi et al. Applied Riemannian geometry to define geodesic paths between nasal curve of different faces. The length of the geodesic path was then used as a similarity measure. The AdaBoost algorithm was used to enhance the authentication performance. They tested their approach on a subset of FRGC v2.0 dataset. Based on their previous work [8-9], Berritti et al. [10] proposed a 3D face recognition approach which represents a 3D face by a set of isogeodesic stripes. A pair of corresponding stripes was matched based on 3D Weighted Walkthroughs (3DWWs). Their experimental results on the FRGC v2.0 dataset was however not satisfactory. The major challenge of this kind of methods is to design an appropriate scheme to extract facial curves/stripes to represent the facial surfaces. Moreover, the selection of the most relevant facial curves/strips to improve the recognition efficiency and accuracy is another important concern.

2) Rigid face recognition: Rigid face recognition is performed on the facial regions which are least affected by facial expressions. Both psychological findings and the 3D face recognition literature reported that the mouth area is

---

* *Corresponding author's* e-mail: 786245423@qq.com

the most affected under facial expressions, while the nose and eyes-forehead areas are less affected. This kind of methods is computationally cheaper and easier to implement. Lei et al. [11] proposed a 3D face recognition approach based on the local low-level geometric features. A facial scan was first divided into three expression - sensitive regions (non-rigid, semi-rigid and rigid), and only the semi-rigid and rigid regions were taken into consideration. Their experimental results showed that the 3D face recognition accuracy was highly influenced by non-rigid facial region. In [12], Mian et al. proposed an approach which automatically segmented the 3D face into different expression-sensitive regions. Based on the semi-rigid facial regions, a matching algorithm, based on Spherical Face Representation (SFR) and Scale-Invariant Feature Transform (SIFT), was combined with a modified ICP algorithm to achieve an efficient 3D face recognition. Chua et al. [13] proposed a 3D face recognition system

based on the point signature features extracted from the rigid parts of the face. They tested their approach on a small dataset with only six individuals and a 100% recognition rate was reported. Chang et al. [14] reported a method named Adaptive Rigid Multiregion Selection (ARMS) for 3D face recognition. The nose area was considered as a rigid facial region due to its relative invariance to facial expressions. Three different overlapping regions were extracted from the rigid region (nose area), and their separate matching scores were combined using the product rule as a similarity measure between different faces.

2.2 SYSTEM OVERVIEW

Figure 1 illustrates the framework of the proposed approach. We briefly describe each block as follows:
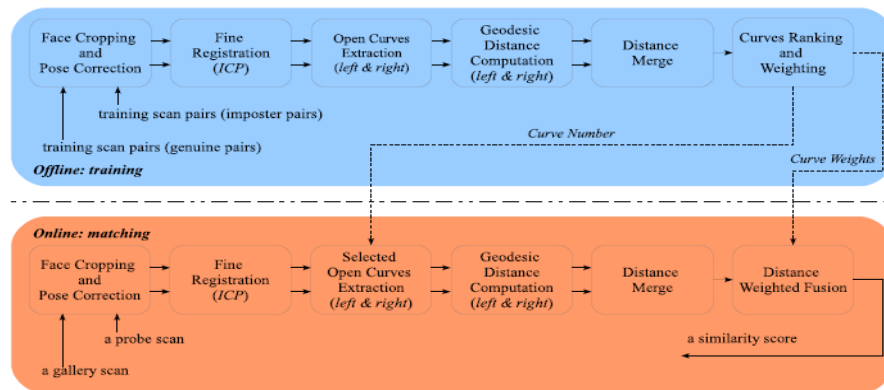

FIGURE 1 Block diagram of the proposed approach

First, a facial scan pre-processing method is performed (Section 3.1), which can automatically perform face cropping and pose correction along with a fine registration between a gallery and a probe face. Then we horizontally partition the pre-processed 3D face into upper and lower regions, and we only take into account the upper region of the face. We further subdivide the upper region into upper-left and upper-right sub-regions with the aim to overcome the potentially non-symmetrical facial problem caused by facial expressions (Section 3.2). Indexed open geodesic curves are collected from both the upper-left and upper-right sub-regions respectively. They are defined by a collection of vertices extracted from a facial mesh with the same geodesic length from a fixed reference vertex (the nosetip is used in our case). Our face matching approach compares different facial shapes by comparing their corresponding curves from the upper-left and upper-right respectively and fusing the pair of their similarity scores. Then, a novel open curve analysis algorithm which fuses the geodesic and the Euclidean distances is used as a similarity score to compare a pair of open geodesic curves (Section 3.3). We also propose a curve ranking and weighting algorithm performed during a training phase to select the most relevant curves to extract during the test

phase, and to assign different weights to the selected ones (Section 3.4). Finally, the curve distances produced by the selected curves are fused according to their ranking weights and used as a matching score between a gallery and a probe face (see Section 3.5).

3 Proposed approach

3.1 FACIAL SCAN PRE-PROCESSING

The largest publicly available 3D face dataset, FRGC v2.0 [15] is used to test our proposed approach. A 3D facial scan in such dataset is represented by a set of dense point-clouds, most of which require pre-processing (as they contain holes, spikes and their poses are not necessarily frontally). An automatic pre-processing is employed which removes spikes, fills in the holes, uniformly samples the point clouds and aligns the faces along principal directions. Initially, the spikes are removed by reducing outlier vertices according to the statistical information of the neighboring vertices. Then a mean value filter is used to smooth the facial surface. The holes are filled-in by using a bi-cubic interpolation. The resulting pointclouds are uniformly sampled at a resolution of 1 mm onto a square grid to achieve a range image representation. The

Hou Xuexian , Zhou Xinzhi , Lei Yinjie

nosetip is automatically detected from the range image using a training free nosetip detection algorithm which was modified from our previous work [16]. The range image is converted back to the pointcloud format and a sphere of radius $r = 80mm$ is used to crop the face. The pose of the cropped face is aligned along automatically computed principal directions using the method proposed in [12]. Figure 2 shows some of the pre-processing results.
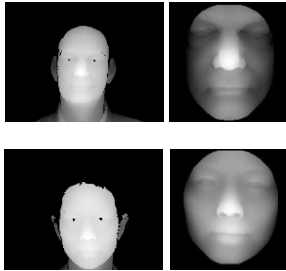

FIGURE 2 Example of 3D facial scans before and after automatic cropping and pose correction.

FIGURE 3 Face fine registration

Next, we finely register the gallery scan with the probe scan and align their nosetip. As a result, even if the final nosetip of the two scans do not correspond to the actual nosetip locations, the two scans are superimposed resulting in the extraction of comparable open geodesic curves. We use two binary masks (see 1st row of Figure 3) to crop the semi-rigid regions of a gallery and probe scan respectively (the larger one is used for gallery and the smaller one is used for the probe in order to avoid incorrect correspondences at the borders). Next we convert the cropped parts into pointclouds and apply the ICP algorithm to find the rigid transformation from the probe scan to the gallery scan. We then apply the calculated rigid transformation to the complete probe face. Finally, we use the nosetip location of the gallery scan to update the nosetip location of the probe scan.

3.2 OPEN CURVE BASED FACIAL REPRESENTATION

We horizontally partition a facial surface into two regions, i.e. the lower and an upper (non-rigid and semi-rigid), with respect to the location of the detected nosetip. We however only take into account the upper region from which we extract a set of indexed open geodesic curves. An appropriate choice of the interval between the curves and the number of curves can provide distinctive features of the facial surface. In our case, a step interval of 2mm between open geodesic curves is selected, and a total of 40 levels (1,3,5,…,79mm from the nosetip) are generated. However, a facial surface cannot always be considered to be perfectly symmetric with respect to the nosetip, especially under the deformations caused by facial expressions (e.g. scornful expression). This asymmetry may lead to an unequal contribution of the left and right sides to the scenario of face recognition. As a result, we opted to further partition the open geodesic curves into upper-left and upper-right again according to the location of the nosetip. Consequently, the similarity measure between two facial surfaces can be computed by comparing their corresponding open geodesic curves from the upper-left and the upper-right sub-regions respectively.
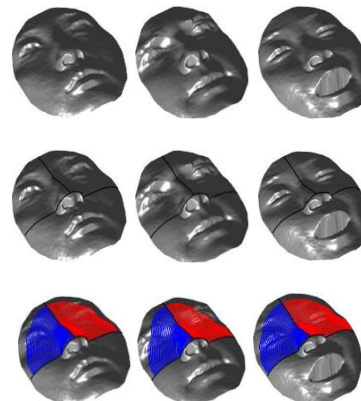

FIGURE 4 Representation of a facial surface by an indexed collection of open geodesic curves

We describe below the steps to extract the open geodesic curves at level $r(r > 0)$ on a given facial mesh.

1) calculate the geodesic distance of all the vertices on the upper region of the given facial mesh (we added 5 additional vertices on each edge of a mesh in order to obtain a smoother geodesic curve);

2) extract the vertices which are at the same level r which results in the extraction of an open geodesic curve O_r;

3) vertically partition O_r into O_r^L and O_r^R (which represent the open geodesic curves from the upper-left and upper-right respectively) with respect to the location of the nosetip;

4) order the extracted curves O_r^L and O_r^R using the Euclidean Minimum Spanning Tree algorithm [17] (we choose the starting points of O_r^L and O_r^R respectively to

be the intersections between O_r^L and O_r^R and the horizontal plane which passes through the nosetip). Figure 4 illustrates examples of the extracted open geodesic curves.

3.3 SHAPES ANALYSIS OF 3D OPEN CURVE

1) Geodesic distance: Recently, Srivastava et al. [18, 19] proposed an efficient method to analyze the shapes of 3D curves as a Riemannian manifold. We will adopt this work to compute a geodesic path between a pair of open geodesic curves and briefly we describe its steps below.

We start by considering an open curve O in R^3, represented by a parametric function $O : [a,b] \rightarrow R^3$. The initial point is $O(a)$ and the final point is $O(b)$, where the interval $U = [a,b]$ is the domain of the curve, and O is an absolutely continuous function on U. In general for an unit interval $U \equiv [0,1]$, $O : U \rightarrow R^3$ is an L_1^2 curve. To analyze the shape of O, we present it mathematically using a Squared-Root Velocity Function (SRVF) [18], denoted by $q(t)$ according to:

$$q(t) = O(t) / \sqrt{\|O(t)\|},\qquad(1)$$

where t is a parameter used to parameterize the open curve ($t \in U$). $\|\cdot\|$ is the R^3 standard Euclidean inner product. The conventional metric to compare the elastic shape of the curves becomes then an L_1^2 metric under this representation. We define a set of open curves in R^3 by:

$$C^O = \{q \in L^2(U,R^3) \mid \int_U \|q(t)\|^2 dt = 1\},\qquad(2)$$

where C^o is the set of all the unit-length open elastic curves in R^3. C^o is called the preshape space, because on which the open curves with the same shape but different orientation and reparameterization can be represented by different elements. In order to impose a Riemannian structure on the preshape space, we consider the tangent space of C^o, which is defined by:

$$T_q(C^o) = \{v \in L^2(U,R^3) \mid \langle v,q \rangle = 0\},\qquad(3)$$

$<v,q>$ denotes the inner product in $L^2(U,R^3)$.

A manifold whose tangent space has an inner product is a Riemannian manifold. In order to define an independent shape, we remove the rotation group $SO(3)$ and the reparameterization group Γ from C^o (see [19] in detail). In the case of C^o, the underlying space is a sphere. For any two points $q_1(t)$ and $q_2(t)$ in C^o, a parameterized geodesic path connecting them is given by $\alpha : U \rightarrow C^o$:

$$\alpha(\tau) = \frac{1}{\sin(\theta)}(\sin(\theta(1-\tau))q_1(t) + \sin(\theta\tau)q_2(t)),\qquad(4)$$

where

$$\alpha(0) = q_1(t), \alpha(1) = q_2(t), \theta = \arccos(< q_1(t), q_2(t) >)$$

is the length of the geodesic path, and τ is used to parameterize the path on the space of curves. Figure 5 shows some examples of the geodesic path on different facial surface. The overall geodesic distance D_g between the curve q_1 and q_2 is given by:

$$D_g = \arccos\!\int_U \langle q_1(t), q_2(t) \rangle dt,\qquad(5)$$

2) Euclidean distance: Different surface shape distributions will generate different open geodesic curves. For a fixed level, the extracted curves from two different facial surfaces (of two different individuals) will be different and distant (when aligned in the 3D Euclidean space) to reflect the difference in the shape distributions of the two faces. This Euclidean distance can therefore be used as another feature for face recognition. More importantly, this Euclidean distance between geodesic curves (at the same level) extracted from two faces of two different individuals will be much more significant than the distance between the curves of the same individual (even under facial expressions).

In some cases, a pair of open geodesic curves from two different faces can be similar in shape (level 55 in Figure 5), which results in a similar geodesic distance. Therefore, the sole use of the geodesic distance by itself is not sufficient for the distinction of the two faces. Consequently, their spatial displacement (Euclidean distance) can be used as an additional feature as illustrated in Figure 5. It shows examples of the spatial displacement of the open geodesic curves between faces of different individuals at three levels (55, 61 and 67).
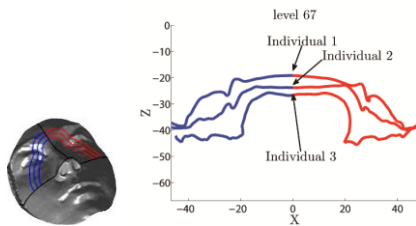
Hou Xuexian , Zhou Xinzhi , Lei Yinjie
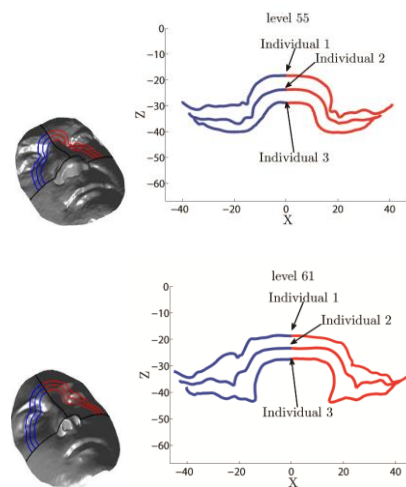
FIGURE 5 Examples of the spatially displacement of the open geodesic curves from different faces at the same level

I	(a) b	(b) c	(c) d	e	3	(d) b	(e) c	d	e
a	0.052	0.013	0.183	0.205	a	0.340	0.113	0.276	0.108
b	–	0.149	0.665	0.061	b	–	0.031	0.100	0.163
c	–	–	0.653	0.503	c	–	–	0.090	0.204
d	–	–	–	0.036	d	–	–	–	0.090
65	b	c	d	e	69	b	c	d	e
a	0.004	0.004	0.006	0.374	a	0.009	0.006	0.014	0.576
b	–	0.005	0.003	0.314	b	–	0.010	0.009	0.572
c	–	–	0.008	0.288	c	–	–	0.017	0.551
d	–	–	–	0.406	d	–	–	–	0.791

FIGURE 6 Face scans and distance values calculated from curves at level 1, 3, 65 and 69

Based on these observations, we use a curve distance D (which fuses the geodesic and Euclidean distances) as a similarity score between two corresponding open geodesic curves extracted from two different faces. Given two open geodesic curves O_1 and O_2, the Euclidean distance D_e between them is computed as:
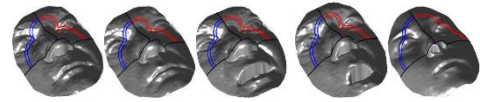
$$D_e = \int_U \sqrt{\|O_1(t) - O_2(t)\|} dt, \qquad (6)$$

Then the curve distance D is obtained by fusing the resulting geodesic distance D_d and the Euclidean distance D_e:

$$D = D_e \cdot D_d, \qquad (7)$$

3.4 CURVE RANKING AND WEIGHTING

Given two facial meshes, according to the open Curve analysis algorithm described in the last section, two curve distances (from the upper-left and the upper-right sub-regions) can be computed respectively, namely $D_L^r 1$ and D_R^r. Then, we combine these two distances by $D^r = D_L^r \cdot D_R^r$, where D^r is the combined curve distance between a pair of open geodesic curves at level r. As a result, 40 level-based curve distances $D^r (r = 1, 2, \ldots, 40)$ between a pair of 3D facial meshes are generated. However, adopting all of the curves for face recognition is unrealistic for the following two reasons. First, some levels of the open geodesic curves from the semi-rigid facial region can also be distorted (although slightly) by facial expressions to a certain extent. Second, some areas exhibit low shape variations from one individual to another (e.g. the local area near the nosetip). Therefore, it is necessary to select curves located in areas that are less affected by facial expressions and which exhibit high shape variations in order to provide an effective distinctive representation for an accurate 3D face recognition system.

An illustrative example is provided in Figure 7, where we compare four levels of open geodesic curves (i.e. level 1, 3, 65 and 69) in order to show their different discriminating power. Five different 3D facial scans are used for this comparison (the first four facial scans are from the same individual, (a) and (b) with neutral expression, (c) and (d) with non-neutral expression).

(e) is a scan of a different individual with neutral expression. The curve distance between any pair of two different scans at a particular level is computed following the algorithm in Section 3.3. These distance values are normalized between 0 and 1 and a smaller value means that such two curves are more similar. These values are reported in the four tables of Figure 6. The first two tables correspond to level 1 and 3. It is shown that the distance values between the curves of the same individual are, at odd, larger than those from different individuals. This clearly demonstrates that level 1 and level 3 curves are not reliable and should be discarded. On the contrast, the tables of level 65 and 69 shows that these levels can robustly discriminate one individual from another and they should therefore be retained.

In the following, we propose a confidence-based algorithm to select the most reliable curves for face recognition. The core of this proposed algorithm is to assign reliability indicators (that we call confidence factors) to each level of facial curves. The curves with top confidence factors are selected and the remaining ones are discarded.

Assume that we have a training set with m faces which belong to n individuals. Each scan from such training set is matched with all of the other facial scans using the curve distance at each of the r levels ($r = 1, 2, \ldots, 40$). A match is genuine if the two scans belong to the same individual, otherwise it is declared as imposter. A matrix $D_{j,k}^r$ which represents the resulting curve distance between the j-th and the k-th facial scans at level r is defined by:

$$D_{j,k}^r \mid \{j \neq k\} = \begin{cases} genuine & \{j,k\} \in n \\ imposter & \{j,k\} \notin n \end{cases} \qquad (8)$$

The imposter matches in $D_{j,k}^r$ are denoted by $F_i^r(\beta)$ where $\beta = 1, \ldots, I$ is the number of total imposter matched while the genuine matches are represented by $F_g^r(\gamma)$, where $\gamma = 1, \ldots, G$ is the number of total genuine matches. Note that, the number of imposter matches (I) is far greater than the number of the genuine ones (G), i.e.

$I \gg G$. A bootstrapping method is then used, starting with all the genuine matches F_g^r and the same number of randomly selected imposter matches, $F_{i,\delta}^r$ (where $\delta = 1,\dots,\eta$), denote by represents the training session number and $\eta = E(I/G)$, and $E(\cdot)$ represents a rounding operator. Next, we keep exchanging $F_{i,\,\delta}^r$ and F_i^r in order to use all of the imposter matches. The confidence factor of the r -th level curve c^r is a measure of its discriminating power and it is evaluated by:

$$c^r = \frac{1}{\eta} \sum_{\delta=1}^{\eta} \frac{((\bar{F}_g^r - \bar{F}_\delta^r)^2 + (\bar{F}_{i,\delta}^r - \bar{F}_\delta^r)^2) \cdot G}{\sum_{\beta=1}^{G}(F_{i,\delta}^r(\beta) - \bar{F}_{i,\delta}^r)^2 + \sum_{\gamma=1}^{G}(F_g^r(\gamma) - \bar{F}_g^r)^2}, \quad (9)$$

where

$$\bar{F}_\delta^r = \frac{1}{2G}(\sum_{\beta=1}^{G} F_g^r(\beta) + \sum_{\gamma=1}^{G} F_{i,\delta}^r(\gamma)),$$

$$\bar{F}_{i,\delta}^r = \frac{1}{G} \sum_{\beta=1}^{G} F_{i,\delta}^r(\beta), \quad (10)$$

$$\bar{F}_g^r = \frac{1}{G} \sum_{\gamma=1}^{G} F_g^r(\gamma),$$

where $\bar{F}_\delta^r$ is the mean value of the matches over all the matches (both imposter and genuine) of the δ -th session, while $\bar{F}_\delta^r$ is the mean value of the genuine matches (it will remain the same during the training process) and $\bar{F}_{i,\delta}^r$ is the mean value of the imposter matches of the δ -th session. We can see that the confidence factor defined in Equation 8 is computed as the average of all the η session of the training. In fact it is defined as the ratio of between-class scatter and within-class scatter (imposter and genuine). Generally, the ratio of the two is an indicator of the discriminating power, i.e. the larger it is the more discriminating the r -th level is.

3.5 CURVE FUSION AND FACE MATCHING

As described in the previous section, a total number of ϕ optimal open curve (with top ϕ confidence factors $\vec{c} = [c^1, c^2, \dots, c^\phi]$) are selected. Next, during the online testing phase, the curve distance is computed between any two 3D scans at each of the selected levels. This results in a similarity matrix $S_r(r = 1,2,\dots,\phi)$ of size $P \times M$ (where P is the number of the gallery faces, and M is the number of the probe faces). S_r at row ω and column p stands for the curve distance between the gallery number ω and the probe number p at the r -th level. A smaller value of $S_r(\omega, p)$ means a higher similarity between the two matched faces. Since different levels of open curves

provide different recognition reliability, the individual similarity matrix S^r is normalized according to a min-max rule before the fusion of the selected curves. Finally, all the elements of the similarity matrix are scaled into a range between 0 and 1:

$$S_r' = \frac{S_r - \min(S_r)}{\max(S_r - \min(S_r)) - \min(S_r - \min(S_r))}, \quad (11)$$

where $\max(S_r)$ and $\min(S_r)$ represent the minimum and maximum values of all the entries in the matrix S_r. The normalized level-based similarity matrices S_r' are then fused to get a combined similarity matrix S. In this work, we use a weighted sum rule for the fusion of all the selected optimal curves as follows:

$$S = \sum_{r=1}^{\phi} \kappa_r S_r',$$

$$\kappa = c^r / \sum_{r=1}^{\phi} c^r, \quad (12)$$

where the fusion weight κ_r for the r -th curve is computed from the confidence factors. The final similarity matrix is again normalized using the min-max rule to normalize each column of the similarity matrix on a range between 0 to 1.

4 Experimental results

4.1 DATASET DESCRIPTION

The training partition of the FRGC v2.0 dataset contains 943 3D facial scans belonging to 273 individuals. In this work, the training partition is used for curve ranking and weighting. The validation partition of FRGC v2.0 has 4007 frontal 3D facial scans of 466 individuals. We select the earliest neutral scan of ever individual to build a gallery of 466 faces and the rest were used as probes for face recognition. For face verification, following the FRGC v2.0 protocols, each facial scan must be matched one-to one with the remaining facial scans (all vs. all). The most challenging standard protocol of FRGC v2.0 (ROC 3) was also tested. We also tested the performance of the proposed approach with another three dataset partition methods (i.e. neutral vs. all, neutral vs. neutral, neutral vs. nonneutral). Another experiment was performed to evaluate the robustness of the proposed approach under severe expression deformations (all of the facial scans with an open mouth as probes).

4.2 OPTIMAL CURVES SELECTION

In this section we aim to experimentally select the most discriminating facial curves using the algorithm in Section 3.4. The confidence factors c^r of each level can be computed, and then a threshold is used to determine the selected curves. Two observations can be made. First, a small threshold will result in the inclusion of less relevant curves that will affect the discriminating power. Second, a high threshold will reduce the number of selected curves

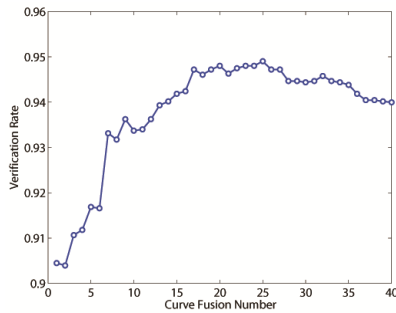and hence will result in an insufficient discriminating power.

FIGURE 7 Selection of optimal facial curves. The accuracy reaches its peak when we select the top 25 curves

This experiment is based on the training partition of FRGC v2.0. In which, the 937 facial scans belonging to 273 individuals are both used as target set and queries, and each scan is matched against all the other ones. We represent this experiment with a selection of different top ϕ curves (ϕ varies from 1 to 40). The Verification Rates (VRs) at 0.1% False Acceptance Rate (FAR) are reported in Figure 7. We can observe that the VR sharply increases when only few curves are used (ϕ less 9). It reaches its peak when the top 25 curves are selected. The VRs then drop when more facial curves are involved. On that basis, we opted to use the top 25 curves in the proposed approach.

4.3 FACE RECOGNITION ON FRGC V2.0 DATASET

1) FRGC v2.0 standard protocols: In order to demonstrate the performance of our curve ranking and weighting algorithm, we performed several experiments using three different curve fusion schemes (top 25, random 25 and last 10). The top 25 scheme is generated as described in Section 4.2. The random 25 scheme means that we randomly select 25 curves from the 40 curves and assign weights to each of them according to their confidence factors. In the last 10 scheme, we use the 10 curves with the lowest confidence factors and their corresponding weights are also assigned to each of them.

We first tested the all vs. all experiment, in which each facial scan from the validation partition is matched with the remaining facial scans. The Receiver Operation Curve (ROC) of this experiment is shown in Figure 9a, and a VR of 91.1% at 0.1% FAR was achieved. The VR achieved for the ROC3 experiment at 0.1% FAR is 93.7%, and the corresponding ROC curve is shown in Figure 9b. Figure 10 illustrate the ROC curves and the Cumulative Match Characteristic (CMC) curves of the proposed approach on the other three dataset partition methods. The VRs at 0.1% FAR for probes with a neutral expression and a nonneutral expression are 99.6% and 97.1% respectively. A 0.1% FAR VR for all the probes (both neutral and nonneutral) is 98.5%. For the identification experiment, we defined galleries and probes as described in Section 4.1.

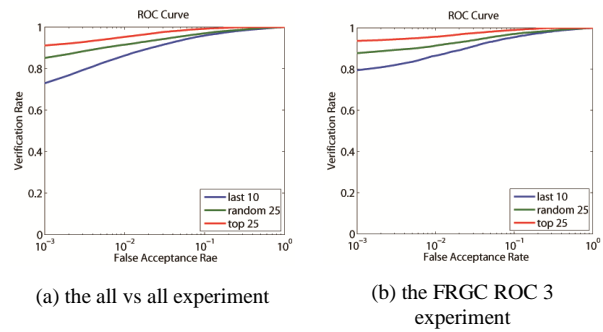(a) the all vs all experiment   (b) the FRGC ROC 3 experiment

FIGURE 8 The ROC curve

The resulting 0.1% FAR VR using top 25 curves are 91.1% and 93.7%, respectively. The rank-1 Identification Rates (IDs) in the case of neutral vs. all, neutral vs. neutral, and neutral vs. nonneutral are 96.7%, 98.7% and 93.9%, respectively.
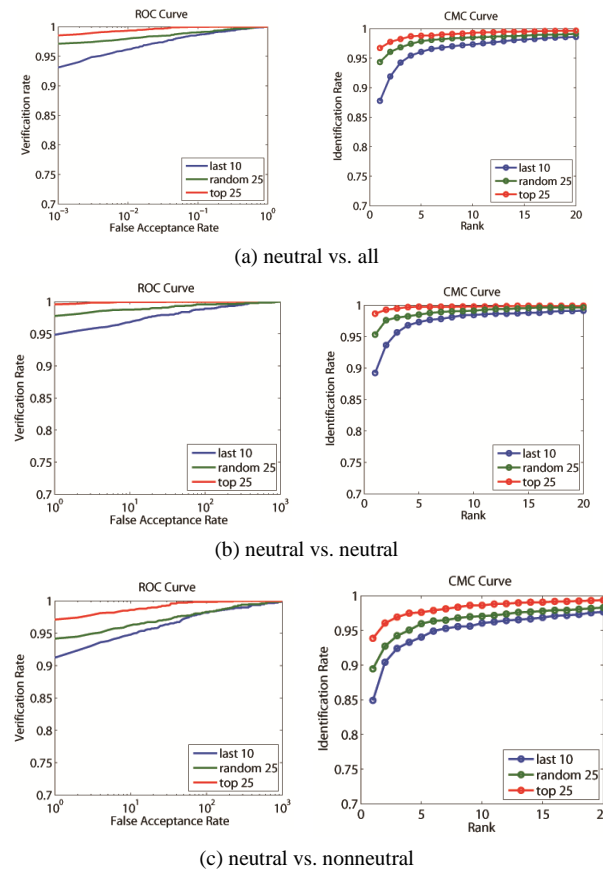

(a) neutral vs. all

(b) neutral vs. neutral

(c) neutral vs. nonneutral

FIGURE 9 3D face recognition results on the FRGC v2.0 dataset.

ROC and CMC curves using different curve fusio in the experiment with neutral faces enrolled. The verification of top 25 for neutral vs. all faces is 98.5% at 0.1% FAR.

We observed that in all of the experiments conducted in this section, the top 25 scheme achieves a significantly greater accuracy compared to the other two curve selection schemes. These results clearly show that the proposed curve ranking and weighting algorithm is effective in selecting the most effective facial curves.
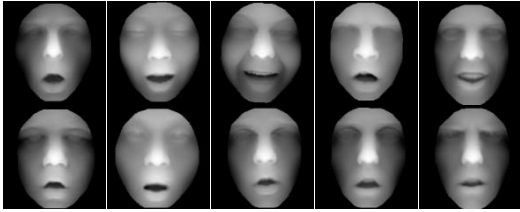
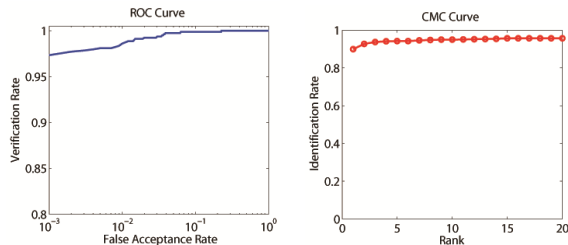FIGURE 10 Examples of the facial scans with an open mouth.

FIGURE11 Recognition results tested with the probes with an open mouth. The 0.1% FAR VR is 97.0% and the rank-1 ID is 90.0%

2) Robustness to large mouth deformations: This Experiment was first proposed by [10] to evaluate the robustness of the proposed approach to large facial expression deformations. Since our approach is based on the extraction of open geodesic curves from the semi-rigid facial regions, it can accommodate severe facial expressions (e.g. with an open mouth). Figure 12 reports the ROC and CMC curves tested using all of the facial scans in the FRGC v2.0 validation partition, with an open mouth, as probes. Compared with the neutral vs. all experiments, the rank-1 ID decreased by 6.7% and the VR at 0.1% FAR decreased by 1.5%. The results of this experiment clearly show that the large facial deformations caused by an open mouth represent a challenge to the face recognition accuracy. However, when dealing with the open mouth probes, our proposed approach still achieved a VR of 97% at 0.1% FAR and a rank-1 ID of 90.0%, which clearly demonstrates the robustness of our proposed approach under large deformations caused by facial expressions.

5 Conclusion

In this work, we proposed a 3D face recognition approach based on the analysis of local open geodesic curves along with a curve ranking and weighting algorithm. We tested the recognition performance of the proposed system on the FRGC v2.0 dataset with different experimental setups. Our experimental results demonstrated the superior performance of the proposed approach: 99.6% and 97.1% VRs at 0.1% FAR for probes with a neutral and a non-neutral expression respectively. The rank-1 IDs under the same conditions were 98.7% and 93.9%. Compared with existing works which were based on the analysis of closed facial curves, this proposed approach is able to deal with large deformations caused by facial expressions. We also achieved a superior result when considering all the probes with an open mouth on FRGC v2.0 dataset.

Acknowledgements

References

[1] Abate a, Nappi M, Riccio D, Sabatino G 2007 2D and 3D face recognition: A survey *Pattern Recognition Letters* **28**(14) 1885-906
[2] Bowyer K, Chang K, Flynn P 2006 A survey of approaches and challenges in 3D and multi-modal 3D+2D face recognition *Computer Vision and Image Understanding* **101**(1) 1-15
[3] Samir C, Srivastava A, Daoudi M 2006 Three-dimentional face recognition using shapes of facial curves *IEEE Transactions on Pattern Analysis and Machine Intelligence* **28**(11) 1858-63
[4] Samir C, Srivastava A, Daoudi M, Klassen E 2009 An intrinsic framework for analysis of facial surfaces *International Journal of computer Vision* **82**(1) 80-95
[5] Dria H, Ben Amor B, Srivastava A, Daoudi M 2009 A Riemannian analysis of 3D nose shapes for partial human biometrics *IEEE International Conference on Computer Vision* 2050-7
[6] Ballihi L, Ben Amor B, Daoudi M, Srivastava A, Aboutajdine D 20.11 Selecting 3D curves on the nasal surface using AdaBoost for person anthentication *in Eurographics Workshop on 3D Object Retrieval* 1-5
[7] ter Haar F, Veltkamp R 2009 A 3D face matching framework for facial curves *Graphical Models* **71**(2) 77-91
[8] Berretti S, Del Bimbo A, Pala P 2006 Description and retrieval of 3D face models using iso-geodesic stripes *in ACM International Workshop on Multimedia Information Retrieval* 13-22
[9] Berretti S, Del Bimbo A, Pala P 2008 Analysis and retrieval of 3D facial models using iso-geodesic stripes *in International Workshop on Content-Based Multimedia Information Retrieval* 257-64

[10] Berretti S, Del Bimbo A, Pala P 2010 3D face recognition using iso-geodesic stripes *in IEEE Transactions on Pattern Analysis and Machine Intelligence* **32**(12) 2162-77
[11] Lei Y, Bennamoun M, Owens R 2013 A structured template based 3D face recognition approach *in International Conference Image and Vision Computing New Zealand ACM* 304-9
[12] Mian A, Bennamoun M, Owens R 2007 An efficient multimodal 2D and 3D hybrid approach to automatic face recognition *IEEE Transactions on Pattern Analysis and Machine Intelligence* **29**(11) 1927-43
[13] Chua C, HanF, Ho Y 2000 3D human face recognition using point signature *IEEE International Conference on Automatic Face and Gesture Recognition, Grenoble France* 233-9
[14] Chang K, Bowyer K, Flynn P 2005 Adaptive rigid multi-region selection for handling expression variation in 3D face recognition *IEEE Conference on Computer Vision and Pattern Recognition* 157-157
[15] Phillips P, Flynn P, Scruggs T, BowyerK, Chang J, Hoffman K, Marques J, Min J, Worek W 2005 Overview of the face recognition grand challenge *IEEE Conference on Computer Vision and Pattern Recognition* 1 947-54
[16] Peng X, Bennamoun M, Mian A 2011 A training-free nose tip detection method from face range images *Pattern Recogntion* **44**(3) 544-58
[17] Shamos M, Hoey D 1975 Closet-point problems *in Annual Symposum on Foundations of Computer Science* 151-62

[18] Joshi S, Klassen E, Srivastava A, Jermyn I 2007 A novel representation for Riemannian analysis of elastic curves in Rn *IEEE Conference on Computer Vision and Pattern Recognition* 1-7

[19] Srivastava A, Klassen E, Joshi S, Jermyn I 2011 Shape analysis of elastic curves in Euclidean spaces *IEEE Transaction on Pattern Recognition and Machine Intelligence* **7**(99) 1415-28

Authors

Xuexian Hou, 22 February, Sichuan Province, China.

Current position, grades: postgraduate student of Sichuan University.
University studies: BSc degree from Ningbo University, Zhejiang, China, in 2012. Currently be pursuing the master's degree with Sichuan University.
Scientific interest: image processing, computer simulation.

Xinzhi Zhou, 13 September, Sichuan Province, China.

Current position, grades: professor with the School of Electronics and Information Engineering Sichuan University.
University studies: BSc and MSc degrees from Chongqing University, Chongqing, PhD degree from Sichuan University, Sichuan, China, in 1988, 1991, and 2003, respectively.
Scientific interest: new sensing technology, intelligent system, and intelligent information processing.

Yinjie Lei, 4 August, Sichuan Province, China.

Current position, grades: a lecturer with the School of Electronics and Information Engineering, Sichuan University.
University studies: BSc and MSc degrees from Sichuan University, Sichuan, PhD degree from University of Western Australia, in 2013.
Scientific interest: image and text understanding, 3D face processing and recognition, 3D modeling, machine learning and statistical pattern recognition.